Designing Self-Sustained Hydrogel Electrolytes for Aqueous, Transparent, and Flexible Batteries

Renan G. Assis,[#,a] Maria K. Ramos [a] and Aldo J. G. Zarbin [,a]*

[a]Departamento de Química, Universidade Federal do Paraná (UFPR), CP 19032, 81531-980 Curitiba-PR, Brazil

The arrival of aqueous sodium-ion batteries has been an essential sustainable advancement in energy storage devices. The use of electrolytes based on polymeric hydrogel is emerging due to the facility in which they can be obtained as film, flexibility, and high ionic conductivity. Additionally, these electrolytes have a dual purpose by acting also as separators. This work deals with the preparation and characterization of hydrogels based on polyvinyl alcohol (PVA), sodium chloride (NaCl), and boric acid (H_3BO_3) to be used as electrolytes in transparent and flexible aqueous sodium-ion batteries. It was observed that lower amounts of NaCl yielded transparent and conductive gels, while increasing the amount of NaCl yielded translucent samples, due to the non-dissolved NaCl. The preparation, gelation step and electrode deposition were optimized to achieve the maximum transparency and conductivity. Subsequently, the selected electrolyte was applied in symmetric devices based on transparent nanocomposite films as electrodes. These devices demonstrated both high transparency and grand current rates. Furthermore, the performance of the electrolyte was verified in a flexible and symmetrical device, revealing an increased current, indicating improved electrode/electrolyte contact. This observation underscores the efficacy of hydrogels in enhancing device performance, particularly in flexible configurations.

Keywords: hydrogel, flexibility, transparency, electrolytes, polyvinyl alcohol

Introduction

Lithium-ion batteries (LIBs) are widely recognized as one of the most prominent rechargeable battery technologies. However, a fundamental challenge in their application concerns security. Safety risks arise from the volatile and flammable organic electrolyte and the reactivity of the electrode material in the formation of dendrites, in addition to being batteries that have a relatively high cost attributed to specialized cell assembly technology (lithium salts and the need for thin electrodes to increase power and energy efficiency).[1-4] Aqueous rechargeable batteries are attractive for large-scale energy storage, offering safety, economics, and sustainability advantages. They eliminate the use of organic solvents, and the ionic conductivities of aqueous electrolytes are higher than the non-aqueous alternatives by approximately two orders of magnitude, ensuring rapid charge/discharge and enhanced round-trip efficiency.[5-7] Moreover, these batteries demonstrate cost-effectiveness with less expensive electrolytic salt and solvent, exemplified by Na^+ in sodium-ion batteries (SIBs), bypassing stringent manufacturing requirements. Additionally, their environmentally friendly nature contributes to high firing efficiency and energy density, even with bulky, scalable electrodes.[8-11]

A growing and vital niche for SIBs is the construction of transparent and flexible devices. Specifically concerning transparency, preparing fully integrated transparent devices remains challenging, given that batteries occupy significant space and volume, and transparent batteries are currently unavailable.[12] The development of technology for creating independent and fully transparent portable devices remains an area of extensive study. It could be a valuable feature for batteries used in integrated photovoltaic devices, smart windows, optical circuits, touch screens, displays, and other applications.[13,14] Concerning flexibility, preparing stable and longstanding bendable devices remains challenging, mainly due to the lack of adequate compressibility and recovery properties during the different bending steps.[15] So, the search for novel materials to be used as electrodes, electrolytes, separators and current collectors, as well as

*e-mail: aldozarbin@ufpr.br
Editor handled this article: Célia M. Ronconi (Associate)
#Present address: Centro de Ciências Naturais e Humanas, Universidade Federal do ABC (UFABC), 09510-580 Santo André-SP, Brazil
In honor of Prof Oswaldo Luiz Alves, for his life dedicated to Chemistry.

the understanding of interfacial bonding between these components, is a critical step on the field. Water evaporation and electrolyte salt precipitation can lead to irreversible degradation in aqueous electrolytes, particularly in separators embedded with liquid electrolytes without proper encapsulation. Unsuitable separator materials can originate problems like limited ionic conductivity (due to inadequate wettability) and electrical shorts between electrodes due to low mechanical strength.[16]

Due to the complexity of integrating new physical, mechanical, and chemical properties into a multifunctional battery, few reports can be found in the literature dealing with transparent and flexible batteries. To achieve success, all the battery components, including active materials, current collectors, electrolytes/separators, and packaging, need to be flexible and transparent, keeping their mechanical resistance and electrochemical functionality,[17] which represents an important scientific challenge. The liquid electrolyte is fully transparent in conventional batteries, whereas the separators, such as fiberglass or polypropylene/polyethylene, are opaque. Consequently, transparent solid electrolytes (such as some gels and polymers) have emerged as the most viable option for transparent batteries, adding the advantage that they are inherently flexible.[18]

Recent studies[19-22] have highlighted hydrogel polymers as promising electrolytes for flexible supercapacitors: they have greater security when compared to liquid electrolytes; unlike dry solid polymer counterparts, the gel polymer electrolytes exhibit higher ionic conductivity in ambient conditions and are easy to fabricate into films of desirable sizes, promoting effective electrode-electrolyte solid contact.

Hydrogels have cross-linked polymer structures featuring interstitial spaces densely filled by water molecules. These hydrogels can retain their dimensional stability as a solid material while accommodating water content of around 2,000 times their original weight, maintaining structural integrity and ionic conductivity.[22] Furthermore, they have charged and/or polar functional groups that make possible to attract and localize electrolytic ions, facilitating their movement through the structure.[22] Several polymeric materials, including polyvinyl alcohol (PVA),[19-26] polyacrylic acid (PAA),[16] polyacrylamide (PAM),[16] and polyvinylidene fluoride,[27] have been assessed as solid electrolytes in energy storage devices. Among these, PVA is a synthetic, thermally stable polymer, commercially available in semicrystalline granular or powder form, derived from the controlled alkaline hydrolysis of polyvinyl acetate.[28,29] PVA is an exceptional electrolyte matrix due to its cost-effectiveness, non-toxicity, chemical stability, high ionic conductivity comparable to liquid electrolytes,

adaptability to a broad pH range, and compatibility with various electrolyte ions.[15,16,20,30] Consequently, it is well known that PVA is easily converted into hydrogels and can serve as a hydrogel electrolyte for electrochemical processes.[16,23,28,31] Harnessing the mechanical properties of PVA, hydrogels can be created through either physical crosslinking, involving a repetitive freezing/thawing process,[15] or chemical methods using crosslinkers like glycerol,[23] sulfuric acid (H_2SO_4),[21] phosphoric acid (H_3PO_4),[26] boric acid (H_3BO_3),[19] and glutaraldehyde.[25] Additionally, aiming for the effectiveness of a hydrogel as an electrolyte, the crosslinking process should be carried out in the presence of an ionic aqueous solution to provide the free ions necessary for charge transport.[19,23] Several formulations of PVA-based hydrogels have been investigated as electrolytes for energy storage applications, and the PVA/KCl/H_3BO_3 combination has proven highly effective as an electrolyte in solid-state supercapacitors.[19] Additional mixtures, such as PVA/NaCl/glycerol[23] and PVA/H_2SO_4/glutaraldehyde[25] have demonstrated successful applications in flexible supercapacitors.

This paper presents the preparation and characterization of different PVA/NaCl/H_3BO_3 hydrogel compositions, exploring various Na^+ concentrations and aiming for transparency, flexibility, and ionic conductivity. The main objective was to find the optimized hydrogel composition, finding the simplest and straightforward process for the gel preparation, allowing the gel integration with various rigid or flexible electrodes in order to be applied simultaneously as electrolytes and separators in energy storage devices. Additionally, the performance of these hydrogels was evaluated in transparent and flexible SIBs. Two methods for integrating electrolytes into electrochemical cells are introduced and optimized to enhance device transparency and electrochemical response. Moreover, transparent and flexible devices using thin films of two nanocomposites (reduced graphene oxide/copper oxide nanoparticles or carbon nanotubes/Prussian blue) were prepared demonstrating the high performance of the optimized hydrogels as both electrolyte and separator.

Experimental

Materials

Polyvinyl alcohol (PVA, polymerization degree 86.5 to 89%, hydrolysis degree 86.5 to 89.5%, Vetec, Duque de Caxias, Brazil), sodium chloride (NaCl, Neon, Lahore, Punjab), boric acid (H_3BO_3, Vetec, Duque de Caxias, Brazil), graphite (90%, Graflake, Nacional de Grafite, São Paulo, Brazil), potassium permanganate ($KMnO_4$, 99%, Synth,

Diadema, Brazil), sulfuric acid (H_2SO_4, 98%, Anidrol, Diadema, Brazil), hydrochloric acid (HCl, 37% Panreac, Castellar del Vallès, Spain), sodium nitrate ($NaNO_3$, Vetec, Duque de Caxias, Brazil), hydrogen peroxide (H_2O_2, 30%, Vetec, Duque de Caxias, Brazil), toluene (99.9%, Sigma-Aldrich, Saint Louis, Missouri, USA and 99%, Neon, Lahore, Punjab), copper nitrate ($Cu(NO_3)_2$, Vetec, Duque de Caxias, Brazil), sodium borohydride ($NaBH_4$, 98%, Acros Organic, Waltham, Massachusetts, USA), potassium chloride (KCl, Vetec, Duque de Caxias, Brazil), and potassium ferricyanide ($K_3[Fe(CN)_6]$, Vetec, Duque de Caxias, Brazil) were used as received. The solutions were prepared with deionized water (18.2 MΩ cm).

Preparation of PVA/NaCl/H₃BO₃ hydrogels

PVA/NaCl/H_3BO_3 hydrogels were prepared through the chemical crosslinking of PVA with H_3BO_3 in the presence of NaCl. Initially, 0.75 g of PVA was dissolved in 10 mL of water under constant stirring and heated at 60 ºC for 20 min. Subsequently, 0.03 g of H_3BO_3 and a known amount of NaCl (0.06; 0.08; 0.12; 0.24 or 0.48 g) were dissolved in 1.5 mL of water. This mixture was then gradually added drop by drop to the PVA solution. Immediately afterward, the resultant mixture was stirred and maintained at 60 °C for 15 min, followed by an additional 10 min of continuous stirring without heat. Finally, the solution was transferred into a plastic Petri dish (5 cm diameter) and allowed to dry at 60 °C for 36 h. The obtained samples will be nominated as PVANa06, PVANa08, PVANa12, PVANa24, and PVANa48, according to the initial amount of NaCl (0.06, 0.08, 0.12, 0.24, or 0.48 g, respectively). Furthermore, control samples were synthesized using the same procedure, but without the incorporation of NaCl or H_3BO_3, or both. These gels will be respectively identified as PVA_H_3BO_3, PVA_NaCl, and PVA.

Electrolyte deposition methods

To enhance the incorporation of PVA/NaCl/H_3BO_3 as a solid electrolyte in electrochemical devices, two methods of hydrogel deposition were assessed (Figure 1): (*i*) just the hydrogel is carefully removed from the dish Petri and sectioned into 1.0 cm × 2.0 cm pieces. For device assembly, a single droplet of water was dispensed onto a previously cleaned indium tin oxide (ITO) electrode (measuring 2.5 × 1.0 cm with a resistivity of 20 Ω square⁻¹). Following this, the hydrogel was positioned over the droplet and compressed by another ITO electrode placed above it (Figure 1a); (*ii*) during the initial hydrogel synthesis, before the gelation process, the mixture was directly applied to the designated ITO electrode, where gelation happened. Starting from ITO electrodes with dimensions of 2.5 cm × 1.0 cm, a tape was affixed to demarcate an area of 2.0 cm × 1.0 cm. Within this specified region, the PVA/NaCl/H_3BO_3 solution was dispensed directly onto the electrode. Different amounts (0.2, 0.35, and 0.5 mL; 4, 7, and 10 drops, respectively) of the solution and different drying times were investigated for PVANa06 and PVANa08 hydrogels to enhance electrochemical properties. Subsequently, at specific intervals, the hydrogel was compressed by another ITO electrode positioned above it (Figure 1b), resulting in the structure ITO/hydrogel/ITO.

Characterization of PVA/NaCl/H₃BO₃ hydrogel films

Fourier transform infrared (FTIR) spectra were obtained in a Fourier transform spectrometer (FTIR, Bruker) from 4000 to 450 cm⁻¹ at room temperature. The Raman spectra were collected on a Witec alpha 300R confocal Raman microscope, with a lateral resolution of 200 nm, a vertical resolution of 500 nm and a 532 nm laser with a resolution of 0.02 cm⁻¹. X-ray diffraction (XRD) analyses were carried
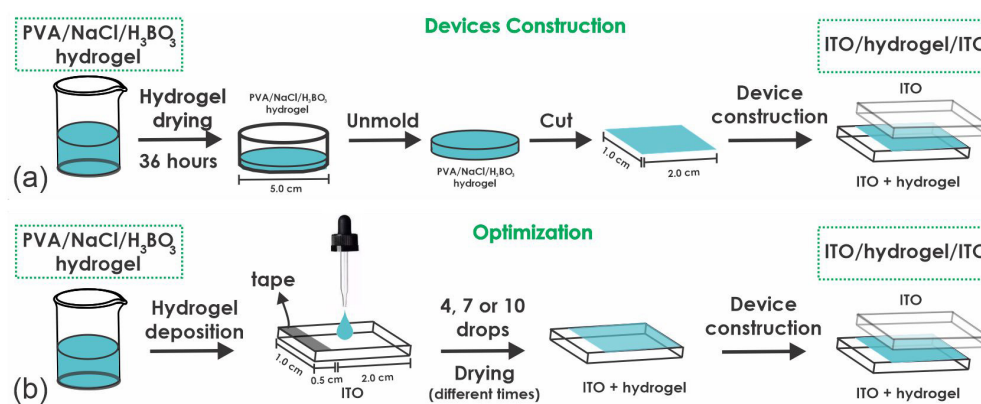
Figure 1. Schematic representation of the different ways in which the electrochemical devices have been prepared: (a) starting from the previously prepared and dried hydrogel; (b) by depositing the gel directly onto a delimited area of an ITO electrode, followed by controlled drying and subsequent sandwiching with another electrode.

J. Braz. Chem. Soc. **2024**, *35*, 11, e-20240086

3 of 12

out in normal mode for powders and shallow angle mode for thin films, both obtained on a Shimadzu XRD-6000 X-ray diffractometer with Cu Kα radiation (λ = 0.15418 nm). Scanning electron microscopy (SEM) images were acquired in a MIRA-3 FEG-SEM Tescan, with a beam at 10 kV at different magnifications and with an energy-dispersive X-ray spectroscopy (EDS) detector (Oxford Instruments) for elemental analysis. UV-Vis spectra were taken directly on the self-supported films on a Shimadzu UV-2450 spectrophotometer. Thermogravimetric analysis (TGA/DSC) was carried out on TA Instruments TG equipment, under synthetic air, at a heating rate of 50 °C min^{-1}. The electrochemical properties of the hydrogel were measured in a μAutolab potentiostat (type III) and an Autolab potentiostat, operated by GPES and NOVA 1.11 software using cyclic voltammetry analysis performed from 0.0 to 0.6 V at different scan rates (5 to 50 mV s^{-1}) in an PVA/NaCl/H$_3$BO$_3$ hydrogels.

Application of PVA/NaCl/H$_3$BO$_3$ hydrogels in electrochemical devices

The PVANa08 hydrogel with optimized volume and time (0.2 mL and 2 h) was applied to electrochemical cells using different nanocomposite thin films deposited on glass/ITO substrates as electrodes. Two different nanocomposites were studied: (*i*) reduced graphene oxide and copper oxide nanoparticles (rGO-CuO) nanocomposites, synthesized by reducing a dispersion of graphene oxide and copper nitrate with sodium borohydride (NaBH$_4$) in a water/toluene liquid/liquid interface, as previously described by us;[32] (*ii*) a carbon nanotube/Prussian blue nanocomposite (CNT-PB), electrochemically synthesized starting from a film of iron- and iron oxide-filled carbon nanotubes in a ferricyanide aqueous solution, according our previous report.[33-38] The preparation of the devices was carried out delineating the electrode area (2.0 cm × 1.0 cm) containing the nanocomposite films. 0.25 mL of the PVANa08 gel were carefully deposited, followed by controlled drying for 2 h and the attachment of a clean ITO, resulting in the formation of the glass-ITO/PVANa08/glass-ITO-rGO-CuO or glass-ITO/PVANa08/glass-ITO-CNT-PB asymmetric devices. Similarly, symmetric devices with the configuration glass-ITO-rGO-CuO/PVANa08/glass-ITO-rGO-CuO and glass-ITO-CNT-PB/PVANa08/ITO-CNT-PB were prepared, starting from the thin films of the nanocomposites as both electrodes. Finally, flexible electrochemical devices were prepared using thin films of rGO-CuO deposited on flexible polyethylene terephthalate/ITO (PET/ITO) as electrodes, in a general configuration of PET-ITO-rGO-CuO/PVANa08/PET-ITO-rGO-CuO.

Results and Discussion

The PVA/NaCl hydrogel cross-links at 60 °C, through the interaction between the boric acid and the hydroxyl groups of the PVA chains, contributing to the enhanced mechanical properties of the hydrogel.[19,21] The 3D networks of cross-linked polymer chains characteristics of hydrogel structure absorb water and swell without dissolving. Gelation involves modifying building blocks, adjusting topological structures, and integrating additives. To be used as ion conductor, the NaCl should be dissolved in the excess of water containing in the porous structure of the reticulated hydrogel. Tuning each element enables these hydrogels to offer high ionic conductivity, electrochemical activity, structural flexibility, and electrolytic permeability, enhancing device performance.[15,22] In the mold casting process, the solution was expeditiously poured into a plastic Petri dish before transitioning into a non-fluid state. Following complete gelation, the resulting free-standing hydrogel film can be effortlessly detached from the Petri dish for subsequent characterization.

Figure 2 presents some structural characterization of the gels as well as their digital photographs (self-standing films, after detaching from the Petri dish, over a text to clarify the visualization, Figure 2A). The samples PVANa06 and PVANa08 exhibited complete transparency, whereas the transparency of the gels decreased and surface roughness increased with increasing NaCl concentration in the samples (PVANa12, PVANa24, and PVANa48), resulting in a translucid material. The thicknesses of the dry gels were measured with a caliper, as 0.1 mm for PVA and PVANa06, 0.2 mm for PVANa08 and PVANa12, and 0.3 mm for PVANa24 and PVANa48. Figure 2B shows the Raman spectra of both pure PVA and PVA/NaCl/H$_3$BO$_3$ hydrogels, characterized by the symmetric and asymmetric stretching modes of CH$_2$ 2910 and 2942 cm^{-1}, respectively.[21,39] The FTIR spectra are illustrated in Figures 2C and 2D. The typical PVA bands are observed at 3300 cm^{-1} (O–H stretching), 2940 cm^{-1} (asymmetric CH$_2$ stretching), 2910 cm^{-1} (symmetric CH$_2$ stretching), 1725 cm^{-1} (C=O, carboxylic acid), 1642 cm^{-1} (δ H$_2$O), 1421 cm^{-1} (CH$_2$ bending), 1327 cm^{-1} (δ OH, involving rocking with CH wagging), 1245 cm^{-1} (σ C–H), 1140 cm^{-1} (shoulder stretching of C–O due to the crystalline portion in PVA), 1090 cm^{-1} (C–O stretching and OH bending due to the amorphous fraction in PVA), 1035 cm^{-1} (C–O stretching vibration of the secondary alcohol (–CH–OH) of PVA), 916 cm^{-1} (CH$_2$ rocking), and 822 cm^{-1} (C–C stretching).[19-21,40] The same bands are presented in all the hydrogel samples spectra, with a single change in the band at 1327 cm^{-1} that was shifted to 1330 cm^{-1} (PVANa06
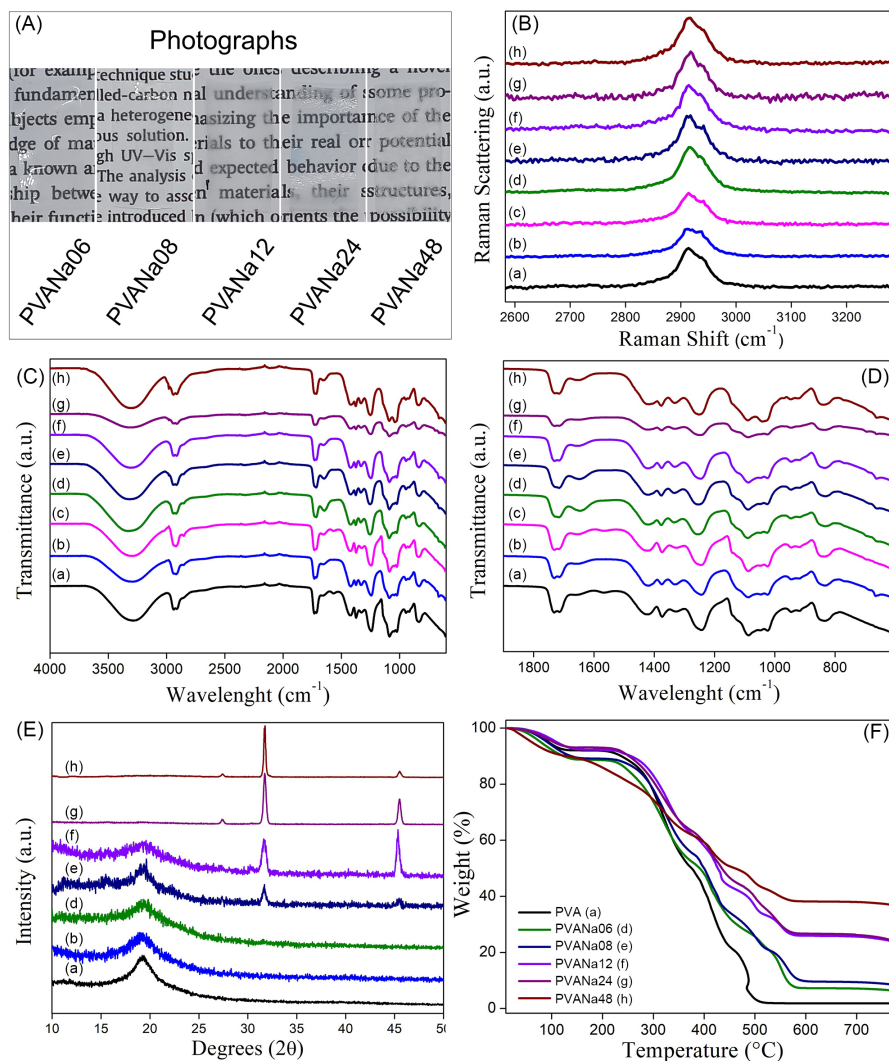
Figure 2. Characterization of the samples: (A) digital photography of PVA/NaCl/H$_3$BO$_3$ hydrogels; (B) Raman spectra; (C,D) FTIR spectra (ATR mode); (E) X-ray diffractometry profile; (F) thermogravimetric curves of samples: (a) black, PVA; (b) blue, PVA_H$_3$BO$_3$; (c) magenta, PVA_NaCl; (d) green, PVANa06; (e) royal, PVANa08; (f) violet, PVANa12; (g) purple, PVANa24; (h) brown, PVANa48.

and PVANa08) and 1333 cm^{-1} (PVANa12, PVANa24, and PVANa48). As this band is directly related to a vibrational mode associated to the OH groups in the PVA chain, this shift can be attributed to an interaction between the boric acid (and the Na$^+$ ions) with these groups.

The XRD patterns of all samples are shown in Figure 2E. A large peak at 19.5° (distance between the crystalline planes (d) = 0.455 nm) can be seen in all samples, corresponding to the crystalline portion of PVA, associated with the planes. Nevertheless, this peak becomes larger and less intense according to the increase of the NaCl content, indicating that the crystallinity of the polymer decreases, as expected. The XRD patterns of the other samples (except for the PVANa06) present also sharp peaks attributed to the fcc NaCl, at 27.4° (111), 31.6° (200), and 45.5° (220).[19,24,41] The NaCl peaks increase in intensity according to the increase of the NaCl in the

initial preparation of the gel, and become predominant in the most concentrated samples. This is indicative that in those samples the initial amount of NaCl exceeded the maximum to be solubilized, remaining as solid crystals embedded into the hydrogel architecture.[20] The presence of these solid crystals is probably the responsible for the non-transparency of those samples (Figure 2A).

Figures 2F and S1 present the thermogravimetric curves of the samples. The PVA presents distinct stages of mass loss: water loss (20 to 140 °C), minor oxygenated functional groups (140 to 350 °C) associated with regions of heightened reactivity and polymer defects, the decomposition the side chain of the PVA (350 to 450 °C), the decomposition of the main chain of PVA (450 to 600 °C). The temperature in which the thermal decomposition of the polymer took place increases in the hydrogels, and increases with the amount of NaCl,

J. Braz. Chem. Soc. **2024**, *35*, 11, e-20240086

5 of 12

indicating that both the cross-linking and the presence of the salt increases the thermal resistance of the polymer. Finally, the presence of boric acid and NaCl in the hydrogels contributes to a residue above 600 ºC, proportional to the initial amount of NaCl (reaching 40% of residue in the sample PVANa48), as expected.

Figures 3 and S2 show the morphology of the films. Specifically, the PVA hydrogel (Figure 3a) comprises a continuous network, showing nodular morphology, as has already been established in previous literature.[42-44] This structure is maintained in the hydrogels prepared with low amount of NaCl (PVANa06, Figure 3b). Otherwise, the increase in the NaCl amount results in non-solubilized (and obviously non-dissociated) NaCl crystals (Figures 3c-3f and S2). This excess of NaCl is expected to not contribute to the ionic conductivity, and they should be responsible for the non-transparence observed in these samples. Energy dispersive spectroscopy (EDS) was used to determine the elemental composition of the samples. The main elements comprising the hydrogels (C, O, B, Na, and Cl) are observed in the EDS spectrum of sample PVANa08. The elemental composition is highlighted in the inset of Figure 3g. The element distribution in the sample PVANa12 can be seen in Figure 3h.

The hydrogels were electrochemically characterized, by cyclic voltammetry, to assess their suitability as electrolytes and separators in devices. In this process, the gels were trimmed to dimensions of 2.0 cm × 1.0 cm and positioned between two ITO electrodes, as illustrated in Figure 4a. This configuration included 0.5 cm on each side to establish a connection between the device and the potentiostat, forming an ITO/hydrogel/ITO structure. Devices created using the hydrogels PVANa06 and PVANa08 exhibited high transparency (Figure 4a). Nevertheless, as the concentration of NaCl was elevated during the hydrogel production, the films become non-transparent, and obviously the same with the devices prepared with them. Cyclic voltammetry measurements were carried out on the devices, as illustrated in Figure 4b at a scan rate of 50 mV s^{-1}, and in Figure S3 (Supplementary Information (SI) section) with varying scan speeds. The voltammograms indicate that the hydrogels display only capacitive current, attributed to forming a double electrical layer (ion accumulation) with the electrode.[23,24] This result is consistent with expectations, as neither the hydrogel nor the ITO electrodes undergo faradaic processes involving electron transfer.[7,45] The PVANa06 hydrogel, with the lowest NaCl concentration in the medium, yields the lowest current. Subsequently,
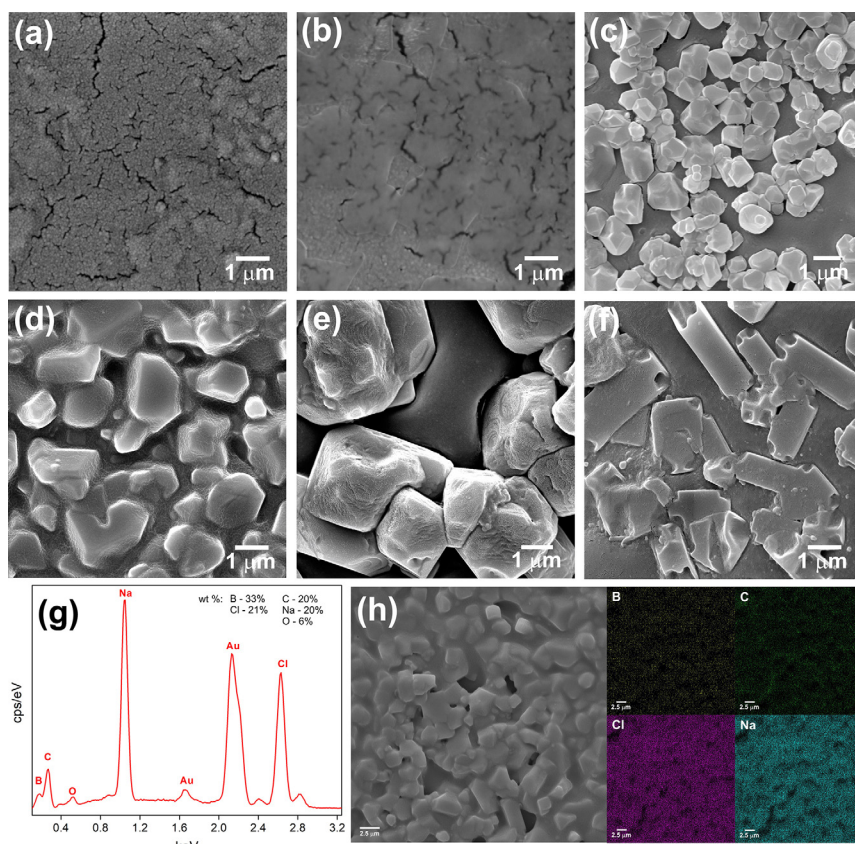
Figure 3. Scanning electron microscopy images of PVA (a), PVANa06 (b), PVANa08 (c), PVANa12 (d), PVANa24 (e), and PVANa48 (f). Representative EDS spectrum of the sample PVANa08 (g); EDS elemental images of the sample PVANa12 (h).

the PVANa08 gel shows a higher current, suggesting a greater availability of Na$^+$ ions for the electrical double-layer process. However, a subsequent decrease in current is observed for the other hydrogels. Notably, PVANa12 and PVANa24 exhibit nearly identical electrochemical currents, followed by another decline for PVANa48. Despite an increase in NaCl concentration, it appears as solid crystals in those samples, non-contributing with the ionic species responsible for the conduction. Otherwise, the presence of the crystals makes the samples more rigid and rough, worsening the contact with the electrodes, and consequently worsening the ionic conductivity. The effect of excess of NaCl is evident in the PVANa48 sample, which exhibits lower current, a less rectangular capacitive profile, and minimal transparency.
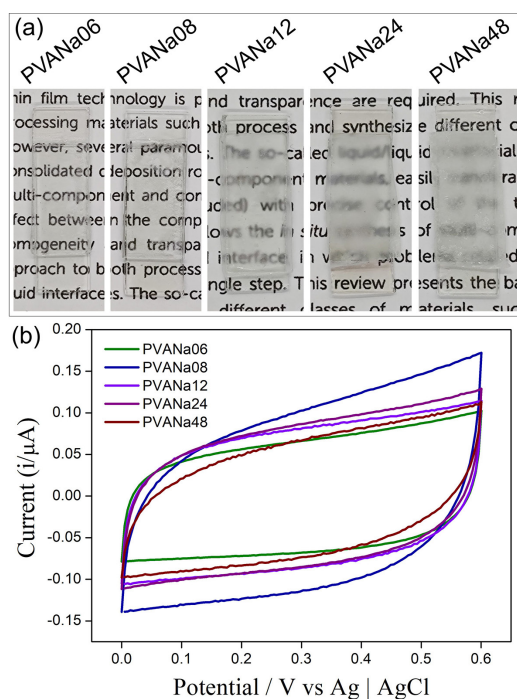
Figure 4. (a) Digital photography of PVANa06, PVANa08, PVANa06, PVANa12, PVANa24, and PVANa48 gel devices configured as ITO/hydrogel/ITO structure; (b) cyclic voltammetry profile of the devices at 50 mV s^{-1}.

In order to optimize the device engineering, we opted for another approach in which the gelation took place directly over the electrode surfaces. This procedure allows the production of highly transparent and flexible hydrogels and enables a close and intimate contact between the electrodes and the hydrogel, minimizing the separation distance between electrodes and thereby reducing diffusion distances. The PVANa06 and PVANa08 hydrogels were chosen for this optimization process due to their transparency and good electrochemical response observed before. So, each solution was individually prepared, and

subsequently, drops of them were dispensed and spread within a defined area marked by tape (2.0 cm × 1.0 cm) directly over the ITO substrate (see Experimental section). The drying times for each hydrogel were optimized following the cyclic voltammetry profiles, as illustrated in Figures 5 and S4. As depicted in Figure S4 (SI section), the drying time emerges as a pivotal and delicate step. In the case of devices assembled with 4 drops (both PVANa06 and PVANa08), a thin film began to develop after 1 h and 20 min of drying. Although the gel exhibited ample consistency to remain adhered to the electrode, each attempt to position the other ITO electrode over the gel and secure it with a clip resulted in the leakage of material, which caused a minor current loss in the electrochemical process, requiring an extended drying period to establish the polymer network and reduce the risk of electrolyte loss during assembly.[21] This way, an optimized time of 2 h yielded the best results for all films prepared with 4 drops of solution, demonstrated by the higher currents for both materials prepared under this condition (Figures S4a-S4d). The assembly of devices with 7 and 10 drops followed a similar rationale. The best drying times of 2 h and 30 min were found for PVANa06 with 7 drops and 4 h for PVANa06 with 10 drops (Figures S4b-S4c). Similarly, PVANa08 devices exhibited optimal results with drying times of 4 h and 20 min for 7 drops and 4 h and 30 min for 10 drops (Figure S4e-S4f).

Following the optimization process (Figure 5), the PVANa06 sample exhibited the most favorable outcome with 10 drops of hydrogel beneath the substrate, requiring 4 h of drying time (Figure 5a-blue). This configuration yielded a significantly higher current when compared to the completely dry hydrogel produced in the initial stage of this study (Figure 5b). In contrast, the PVANa08 sample achieved optimal results after optimization with 4 drops of hydrogel and 2 h of drying (Figure 5c-black), surpassing the current obtained in its initial stage (Figure 5d). In a comparative analysis between the PVANa06-10drops and PVANa08-4drops samples, the superior optimization result was observed for the PVANa08-4drops (Figure 5e). Films with smaller volumes are thinnest, so the PVANa08 prepared with 4 drops is the most efficient among all the experiments described here, because it shows the higher currents and higher transparency. Notably, the PVANa08-4drops sample also exhibited superior optical quality and transparency compared to its completely dry counterpart, PVANa08 (Figure 5f), evidencing the effectiveness of the proposal to prepare the devices based on the gelation directly over the electrodes.

To demonstrate the viability of the concept, we utilized rigid devices featuring thin films nanocomposites deposited over ITO as electrodes, and the optimized

J. Braz. Chem. Soc. **2024**, *35*, 11, e-20240086

7 of 12
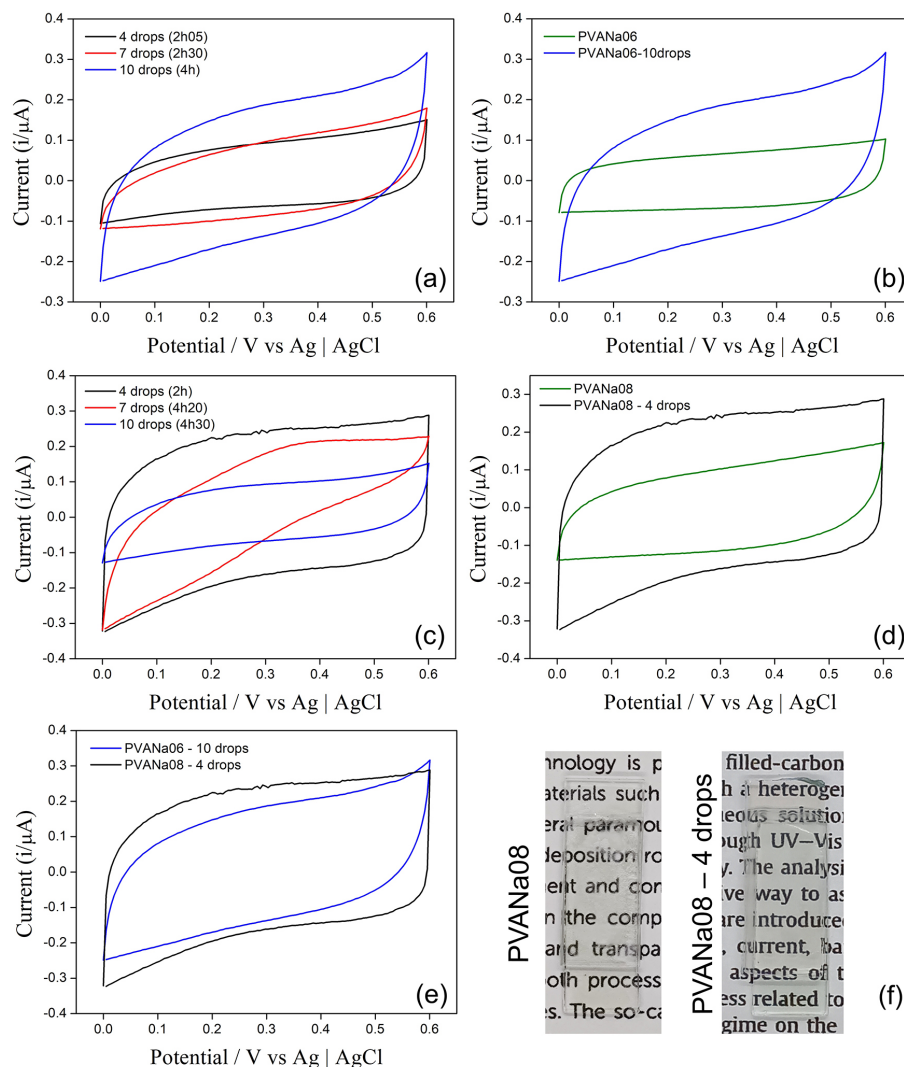
Figure 5. Optimizing the electrochemical performance of PVANa06 (a-b) and PVANa08 (c-d) hydrogels using 4, 7, and 10 drops (0.2, 0.35 and 0.5 mL, respectively) directly over the electrodes, varying the dry times (a/c) and comparing the best optimization results with the completely dry gels obtained initially (b/d) at 50 mV s^{-1}; (e) comparative cyclic voltammetry of devices based on PVANa06-10drops and PVANa08-4drops, at 50 mV s^{-1}; (f) digital photography of the PVANa08 and PVANa08-4drops devices structured as ITO/hydrogel/ITO.

PVANa08 hydrogel (4 drops, deposited directly over the electrodes) as electrolyte. Figures 6a and 6b show the transmittance spectra and the digital images (as insets) of the final devices based on glass-ITO/PVANa08/glass-ITO-CNT-PB (Figure 6a) and glass-ITO-CNT-PB/PVANa08/glass-ITO-CNT-PB (Figure 6b). Both devices present the typical blue color of Prussian blue, and an absorbance band at approximately 700 nm, attributed to the characteristic intervalence band transition of PB.[35-38,43] It is evident by the photography in the insets in Figures 6a and 6b the high homogeneity and transparency of the devices: the glass-ITO/PVANa08/glass-ITO-CNT-PB exhibits a transparency of 50% at 550 nm (without discounting the contribution of glass substrate) and the glass-ITO-CNT-PB/PVANa08/glass-ITO-CNT-PB shows transmittance of 29% at 550 nm. The transparency of the

hydrogel was assessed by depositing four drops of the PVANa08 gel on a quartz substrate, yielding a transparency value of 70% at 550 nm (Figure S5, SI section).

Figure 6c shows the electroactivity of the glass-ITO-CNT-PB/PVANa08/glass-ITO-CNT-PB device, characterized by a well-defined redox couple at E$_{1/2}$ of 0.12 V associated to the Prussian white/Prussian blue (PW/PB) process. This occurrence of this redox pair indicates the presence of a well-defined PB structure and excellent ionic and electronic conductivity of the device.[46,47] For the symmetric glass-ITO-CNT-PB/PVANa08/glass-ITO-CNT-PB device (Figure 6d), the redox processes are overlapped as one electrode are reduced while the other one oxidizes at the same potential. Despite the less distinct definition of redox peaks, this device exhibits a higher current rate, demonstrating the facile Na$^+$ intercalation processes within
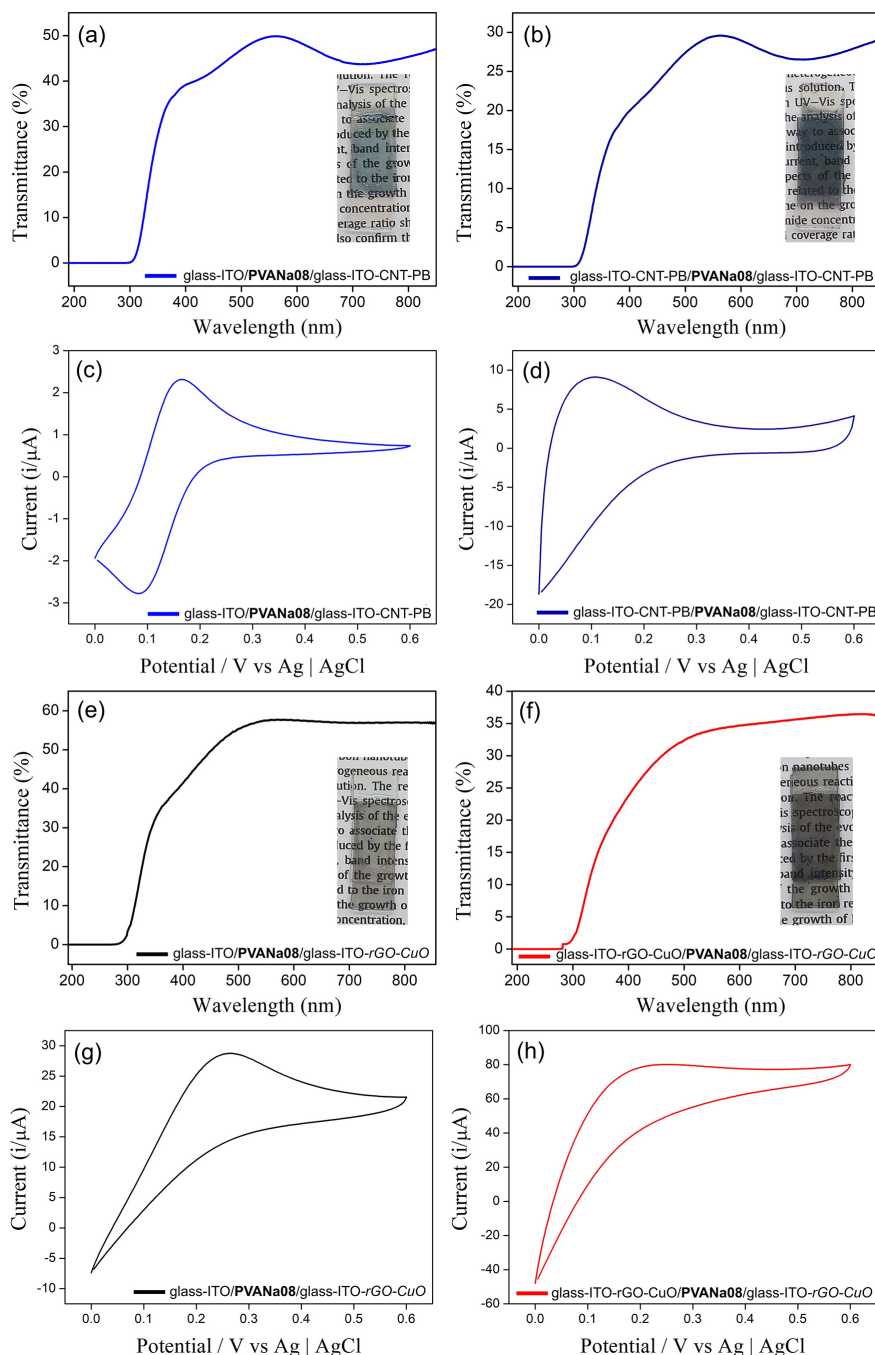
Figure 6. Optical and electrochemical properties of the devices prepared with the PVANa08 (4 drops, 2 h drying): (a,b,e,f) transmittance spectra (photographic images of the devices as insets); (c,d,g,h) cyclic voltammetry profile (at 50 mV s⁻¹). (a,c) glass-ITO/PVANa08/glass-ITO-CNT-PB; (b,d) glass-ITO-CNT-PB/PVANa08/glass-ITO-CNT-PB; (e,g) glass-ITO/PVANa08/glass-ITO-rGO-CuO; (f,h) glass-ITO-rGO-CuO/PVANa08/glass-ITO-rGO-CuO.

the PB structure promoted by the PVANa08d hydrogel.

The transmittance spectra and the digital photographs of the rGO-CuO-based devices are shown in Figures 6e and 6f. The optical images (insets, Figures 6e and 6f) exhibit by high homogeneity and a gray color typical of rGO. A transparency of 57% at 550 nm is observed for the glass-ITO/PVANa08/glass-ITO-rGO-CuO, going to 34% at 550 nm for the glass-ITO-rGO-CuO/

PVANa08/glass-ITO-rGO-CuO. The electroactivity of the rGO-CuO-based devices are illustrated in Figures 6g and 6h, characterized by an oxidation peak at cyclic voltammogram at $E = 0.25$ V due to the Cu^+/Cu^{2+} process.[48]

The results summarized in Figure 6 are precise concerning the viability of applying the hydrogels prepared in this work as electrolytes in real aqueous Na-ion battery devices. Remarkably, the current rates

J. Braz. Chem. Soc. **2024**, *35*, 11, e-20240086

9 of 12

are higher, even when compared to the same electrodes in a conventional three-electrodes electrochemical cell in aqueous solution of NaCl.[46] The transparency is promising, even higher than the 22% obtained on similar devices using a physical separator and liquid electrolyte.[14] The optimized process to prepare the hydrogel described here yielded an exceptionally thin electrolyte that also acts as separator. A thin separator reduces the distance between electrodes, facilitating ion diffusion and increasing the conductivity while offering high transparency (70%). Additionally, the use of these gels prevents outcomes such as bubble formation or electrolyte leakage, commonly associated with liquid electrolytes.

Finally, we investigated the preparation of flexible devices based on the hydrogels, repeating the ITO-rGO-CuO/PVANa08/ITO-rGO-CuO configuration, but now using an ITO film deposited over PET as substrate (device PET-ITO-rGO-CuO/PVANa08/PET-ITO-rGO-CuO). The picture of the device, as well as its cyclic voltammetry profile after different cycles of twist and bending, are shown in Figure 7. The images illustrate how the films adhere together without additional clips, allowing for easy device twisting without disrupting the connection. Furthermore, electrochemical measurements conducted on the devices reveal an increase in current when the ends are twisted upwards and even greater current when the ends are twisted in opposite directions. This observation indicates that as the electrodes are twisted, the separating gel is accommodated with the electrodes, leading to a more intimate contact and an enhanced electrochemical response. The remarkable advantage of hydrogels lies in their suitability as separators/electrolytes in flexible devices. Unlike liquid electrolytes, which are unsuitable for experiments involving bending, these gels adapt to the shape of the electrode and can be manipulated easily without losing properties, often even enhancing the final response.
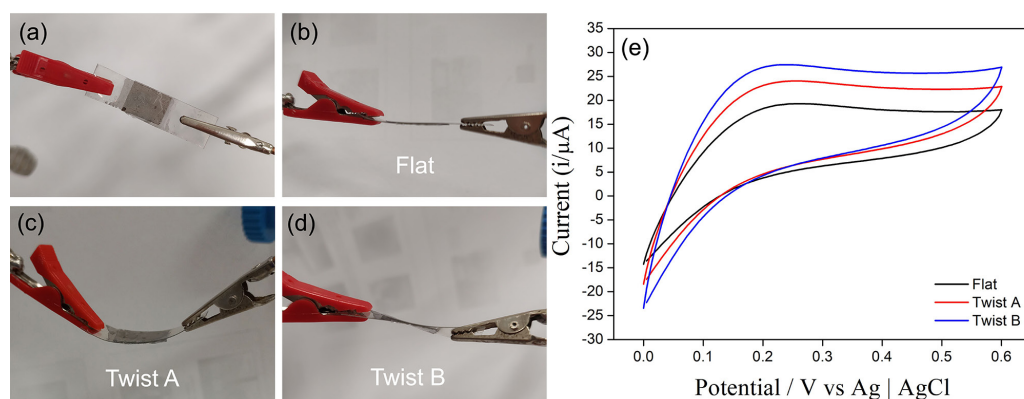
Conclusions

In conclusion, we demonstrated the preparation of self-supporting films of hydrogels comprising PVA/NaCl/H_3BO_3 using different NaCl concentration, in which some compositions yielded films with high transparency, low roughness and high ionic conductivity. Afterwards, we introduced and optimized a direct approach for incorporating the hydrogel in devices that involves the meticulous control of the gelation process directly over the surface of the electrodes. This method led to faster and more straightforward device preparation, taking only 2 to 4 h (including hydrogel preparation, drying, and assembly), while achieving greater transparency and significantly higher current compared to the traditional electrode-electrolyte sandwiching method. To assess the practicality of our optimized hydrogel formulation, we evaluated rigid and flexible symmetric devices with nanostructured thin films as electrodes. These devices exhibited high transparency and current rates, with no current loss during twisting, surpassing similar devices prepared with liquid electrolytes. The results presented here open a great avenue for the utilization of the optimized hydrogel formulation in different kind of devices, mainly transparent, flexible, aqueous Na-ion batteries. However, other devices that require ionic conductivity, transparency and flexibility can also benefit from this material, which further expands the possibility of technological application.

Supplementary Information

Supplementary data (TGA of control samples, SEM images in different magnifications, cyclic voltametric data and UV-Vis spectra of hydrogel) are available free of charge at http://jbcs.sbq.org.br as PDF file.

Figure 7. Digital photographs of the flexible PET-ITO-rGO-CuO/PVANa08/PET-ITO-rGO-CuO device flat and twisted in two different ways (a-d) and their respective cyclic voltammetry at 50 mV s^{-1} (e).

Author Contributions

Renan G. Assis was responsible for conceptualization, visualization, methodology, writing original draft; Maria K. Ramos for conceptualization, visualization, methodology, formal analysis, writing original draft, review and editing; Aldo J. G. Zarbin for conceptualization, funding acquisition, methodology, project administration, resources, supervision, validation, writing review and editing.

References

1. Kim, H.; Hong, J.; Park, K. Y.; Kim, H.; Kim, S. W.; Kang, K.; *Chem. Rev.* **2014**, *114*, 11788. [Crossref]

2. Bin, D.; Wang, F.; Tamirat, A. G.; Suo, L.; Wang, Y.; Wang, C.; Xia, Y.; *Adv. Energy Mater.* **2018**, *8*, 1703008. [Crossref]

3. Tang, W.; Zhu, Y.; Hou, Y.; Liu, L.; Wu, Y.; Loh, K. P.; Zhang, H.; Zhu, K.; *Energy Environ. Sci.* **2013**, *6*, 2093. [Crossref]

4. Ramos, M. K.; Zarbin, A. J. G. In *Materials Nanoarchitectonics*; Ariga, K.; Azzaroni, O., eds.; Elsevier: city, ch. 10, p. 207. [Crossref]

5. de La Llave, E.; Borgel, V.; Park, K. J.; Hwang, J. Y.; Sun, Y. K.; Hartmann, P.; Chesneau, F. F.; Aurbach, D.; *ACS Appl. Mater. Interfaces* **2016**, *8*, 1867. [Crossref]

6. Lee, H.-W.; Pasta, M.; Wang, R. Y.; Ruffo, R.; Cui, Y.; *Faraday Discuss.* **2014**, *176*, 69. [Crossref]

7. Mathis, T. S.; Kurra, N.; Wang, X.; Pinto, D.; Simon, P.; Gogotsi, Y.; *Adv. Energy Mater.* **2019**, *9*, 1902007. [Crossref]

8. Huang, S.; Zhu, J.; Tian, J.; Niu, Z.; *Chem. - Eur. J.* **2019**, *25*, 14480. [Crossref]

9. Fang, G.; Zhou, J.; Pan, A.; Liang, S.; *ACS Energy Lett.* **2018**, *3*, 2480. [Crossref]

10. Liu, J.; Xu, C.; Chen, Z.; Ni, S.; Shen, Z. X.; *Green Energy Environ.* **2018**, *3*, 20. [Crossref]

11. Dong, C.; Xu, F.; Chen, L.; Chen, Z.; Cao, Y.; *Small Struct.* **2021**, *2*, 2100001. [Crossref]

12. Yang, Y.; Jeong, S.; Hu, L.; Wu, H.; Lee, S. W.; Cui, Y.; *Proc. Natl. Acad. Sci. U. S. A.* **2011**, *108*, 13013. [Crossref]

13. Kwon, O.; Hwang, H. J.; Ji, Y.; Jeon, O. S.; Kim, J. P.; Lee, C.; Shul, Y. G.; *Sci. Rep.* **2019**, *9*, 3175. [Crossref]

14. Husmann, S.; Ramos, M. K.; Zarbin, A. J. G.; *Electrochim. Acta* **2022**, *422*, 140548. [Crossref]

15. Liu, Z.; Zhang, J.; Liu, J.; Long, Y.; Fang, L.; Wang, Q.; Liu, T.; *J. Mater. Chem. A* **2020**, *8*, 6219. [Crossref]

16. Wang, Z.; Li, H.; Tang, Z.; Liu, Z.; Ruan, Z.; Ma, L.; Yang, Q.; Wang, D.; Zhi, C.; *Adv. Funct. Mater.* **2018**, *28*, 1804560. [Crossref]

17. Wehner, L. A.; Mittal, N.; Liu, T.; Niederberger, M.; *ACS Cent. Sci.* **2021**, *7*, 231. [Crossref]

18. Sun, N.; Sun, H.; Tan, D.; Guo, Q.; Zhang, Z.; Tao, Z.; Fang, C.; Bu, J.; Huang, J.; Jiang, C.; *Chem. Eng. J.* **2023**, *469*, 143997. [Crossref]

19. Sun, K.; Feng, E.; Zhao, G.; Peng, H.; Wei, G.; Lv, Y.; Ma, G.; *ACS Sustainable Chem. Eng.* **2019**, *7*, 165. [Crossref]

20. Pavani, Y.; Ravi, M.; Bhavani, S.; Sharma, A. K.; Rao, V. V. R. N.; *Polym. Eng. Sci.* **2012**, *52*, 1685. [Crossref]

21. Wang, K.; Zhang, X.; Li, C.; Sun, X.; Meng, Q.; Ma, Y.; Wei, Z.; *Adv. Mater.* **2015**, *27*, 7451. [Crossref]

22. Guo, Y.; Bae, J.; Zhao, F.; Yu, G.; *Trends Chem.* **2019**, *1*, 335. [Crossref]

23. Peng, S.; Jiang, X.; Xiang, X.; Chen, K.; Chen, G.; Jiang, X.; Hou, L.; *Electrochim. Acta* **2019**, *324*, 134874. [Crossref]

24. Hu, X.; Fan, L.; Qin, G.; Shen, Z.; Chen, J.; Wang, M.; Yang, J.; Chen, Q.; *J. Power Sources* **2019**, *414*, 201. [Crossref]

25. Bai, Y.; Liu, R.; Liu, Y.; Wang, Y.; Wang, X.; Xiao, H.; Yuan, G.; *Sci. China Chem.* **2021**, *64*, 852. [Crossref]

26. Yu, D.; Goh, K.; Wang, H.; Wei, L.; Jiang, W.; Zhang, Q.; Dai, L.; Chen, Y.; *Nat. Nanotechnol.* **2014**, *9*, 555. [Crossref]

27. Hao, J.; Xiao, Q.; Lei, G.; Li, Z.; Wu, L.; *Electrochim. Acta* **2014**, *125*, 450. [Crossref]

28. Nagarkar, R.; Patel, J.; *Acta Scientific Pharm. Sci.* **2019**, *3*, 34. [Link] accessed in May 2024

29. Wu, F.; Lin, X.; Xu, Y.; Zhang, D.; He, Y.; Liu, M.; *Sci. China Mater.* **2023**, *66*, 4782. [Crossref]

30. Zeng, L.; Liu, B.; Gao, G.; *Sci. China Mater.* **2023**, *66*, 4062. [Crossref]

31. Aslam, M.; Kalyar, M. A.; Raza, Z. A.; *Polym. Eng. Sci.* **2018**, *58*, 2119. [Crossref]

32. Ramos, M. K.; Zarbin, A. J. G.; *Appl. Surf. Sci.* **2020**, *515*, 146000. [Crossref]

33. Schnitzler, M. C.; Oliveira, M. M.; Ugarte, D.; Zarbin, A. J. G.; *Chem. Phys. Lett.* **2003**, *381*, 541. [Crossref]

34. Schnitzler, M. C.; Zarbin, A. J. G.; *J. Solid State Chem.* **2009**, *182*, 2867. [Crossref]

35. Husmann, S.; Lima, L. F.; Roman, L. S.; Zarbin, A. J. G.; *ChemSusChem* **2018**, *11*, 1238. [Crossref]

36. Husmann, S.; Orth, E. S.; Zarbin, A. J. G.; *Electrochim. Acta* **2019**, *312*, 380. [Crossref]

37. Husmann, S.; Zarbin, A. J. G.; *Electrochim. Acta* **2018**, *283*, 1339. [Crossref]

38. Ferreira, C. M.; Ramos, M. K.; Zarbin, A. J. G.; *Eur. J. Inorg. Chem.* **2021**, *2021*, 3373. [Crossref]

39. Marka, S. K.; Sindam, B.; James Raju, K. C.; Srikanth, V. V. S. S.; *RSC Adv.* **2015**, *5*, 36498. [Crossref]

J. Braz. Chem. Soc. **2024**, *35*, 11, e-20240086

11 of 12

40. Jipa, I. M.; Stoica, A.; Stroescu, M.; Dobre, L. M.; Dobre, T.; Jinga, S.; Tardei, C.; *Chem. Pap.* **2012**, *66*, 138. [Crossref]

41. Rabiei, M.; Palevicius, A.; Dashti, A.; Nasiri, S.; Monshi, A.; Vilkauskas, A.; Janusas, G.; *Materials* **2020**, *13*, 4380. [Crossref]

42. An, Q.; Li, F.; Ji, Y.; Chen, H.; *J. Memb. Sci.* **2011**, *367*, 158. [Crossref]

43. Luo, X.; Li, J.; Lin, X.; *Carbohydr. Polym.* **2012**, *90*, 1595. [Crossref]

44. Al-Gorair, A. S.; Hawsawi, H.; Fawzy, A.; Sobhi, M.; Alharbi, A.; Hameed, R. S. A.; El Wanees, S. A.; Abdallah, M.; *Int. J. Electrochem. Sci.* **2021**, *16*, 211119. [Crossref]

45. Sharma, P.; Bhatti, T. S.; *Energy Convers. Manage.* **2010**, *51*, 2901. [Crossref]

46. Nossol, E.; Zarbin, A. J. G.; *J. Mater. Chem.* **2012**, *22*, 1824. [Crossref]

47. Husmann, S.; Zarbin, A. J. G.; Dryfe, R. A. W.; *Electrochim. Acta* **2020**, *349*, 136243. [Crossref]

48. Ramos, M. K.; Martins, G.; Marcolino-Junior, L. H.; Bergamini, M. F.; Oliveira, M. M.; Zarbin, A. J. G.; *Mater. Horizons* **2023**, *10*, 5521. [Crossref]